

## Physics of Penetration of Resonant Magnetic Perturbations Used for Type I Edge Localized Modes Suppression in Tokamaks.

M. Bécoulet<sup>(1)</sup>, G. Huysmans<sup>(1)</sup>, X. Garbet<sup>(1)</sup>, E. Nardon<sup>(2)</sup>, M. Schaffer<sup>(3)</sup>, A. Garofalo<sup>(3)</sup>, K. Shaing<sup>(4-5)</sup>, A. Cole<sup>(4)</sup>, J.-K. Park<sup>(6)</sup>, P. Cahyna<sup>(7)</sup>.

<sup>1</sup>Association Euratom-CEA, IRFM, Cadarache, 13108, St-Paul-lez-Durance, France.

<sup>2</sup>Euratom/UKAEA Fusion Association, Culham Science Centre, Abingdon, OX143DB, U.K.

<sup>3</sup>General Atomics, P.O. Box 85608, San Diego, CA 92186-5688, USA.

<sup>4</sup>University of Wisconsin, Madison, WI53706-1609, USA.

<sup>5</sup>Plasma and Space Science Center and Physics Department, National Cheng Kung University, Tainan, Taiwan 70101, Republic of China.

<sup>6</sup>Princeton Plasma Physics Laboratory, Princeton, NJ 08543, USA.

<sup>7</sup>Association EURATOM/IPP.CR, Prague, Czech Republic.

e-mail contact of main author: marina.becoulet@cea.fr

**Abstract.** Non-linear reduced MHD modelling of the response of a toroidally rotating plasma on Resonant Magnetic Perturbations (RMPs) is presented for DIII-D and ITER typical parameter. The non-linear cylindrical reduced MHD (RMHD) code was adapted to take into account toroidal rotation and plasma braking mechanisms such as resonant braking and the Neoclassical Toroidal Viscosity (NTV). The resonant harmonics ( $q = m/n$ ) penetration time to the pedestal top ( $r \sim 0.9$ ) is estimated  $\sim 600ms$  for ITER and  $\sim 60ms$  for DIII-D. Numerical modelling shows that the effective screening of the magnetic islands by plasma rotation is larger for stronger rotation and lower resistivity ( $\psi_{nm}^{plas} / \psi_{nm}^{vac} \sim \eta^{5/6} / V_{tor}$ ). The non-resonant helical harmonics ( $q \neq m/n$ ) do not produce magnetic islands, penetrate on Alfvén-like time, are not screened by plasma rotation, but produce NTV. The modelling demonstrated that the central islands are screened by rotation and that the pedestal region ( $r > 0.9$ ) is expected to be ergodic both in DIII-D and ITER. If the “1/v” low collisionality NTV regime is dominant in ITER, as it is suggested by dedicated DIII-D experiments and modelling, a counter (with respect to the plasma current) rotation is predicted for ITER.

### 1. Introduction.

During the recent design review of ITER, Type I Edge Localised Mode (ELM) control was identified as a high priority task [1]. One of the promising methods to control Type I ELMs is the installation of dedicated coils that achieve this goal by modifying the edge magnetic field, so called Resonant Magnetic Perturbations (RMP) coils. RMPs have been shown to be effective in eliminating Type I ELMs in DIII-D [2] or significantly mitigating them [3] in JET. At present, ELM control by RMP is recommended for ITER since it could increase the lifetime of the ITER divertor by reducing heat and particle fluxes due to Type I ELMs and hence reducing surface erosion [1]. Present day experiments on ELM control by RMP are not completely understood. The extrapolations to ITER are mainly based on an empirical criterion and “vacuum” field modelling suggesting that ELMs are suppressed when the edge plasma is ergodized in the pedestal region for  $\sim \sqrt{\psi} > 0.9$ . This criterion is also used for the design of the RMP coils for ITER [4,5]. However, depending on the plasma parameters and the RMP spectrum, the actual RMP field could be very different, especially in rotating plasmas where the generation of the current perturbations near rational surfaces could prevent reconnection leading to the effective screening of RMPs [6]. It is known from experiment that helical magnetic perturbations can significantly influence the toroidal rotation [2-3,8-10]. In most experimental cases slowing down of the global plasma rotation is observed potentially leading to core MHD and modes locking [3,8-10]. However, in some [2]

experiments an increase of the toroidal rotation at the pedestal was observed and, moreover, at weak co- and counter rotation an acceleration in the counter direction was demonstrated [10]. The Neoclassical Toroidal Viscosity (NTV), resulting from the toroidal drag force experienced by the plasma particles moving along field lines distorted by helical magnetic perturbations [11-13], was proposed as a possible mechanism for the global plasma braking. The helical perturbations can appear due to the intrinsic MHD activity (Resistive Wall Modes, tearing modes etc.) or external magnetic perturbations such as RMPs. NTV is produced due to any helical magnetic perturbation including both resonant ( $q=m/n$ ) the non-resonant part ( $q \neq m/n$ ) of the perturbation spectrum [8-9,11-13]. The understanding of the rotating plasma response on RMPs is important in the optimization of the RMP coils spectrum. The loss of the plasma co-rotation due to NTV can be important in ITER, where the expected toroidal rotation is slow ( $\sim 1\text{kHz}$ ) compared to the existing experiments ( $\sim 10\text{kHz}$ ) [2,3,10]. This paper describes recent results based on the non-linear reduced MHD modelling of RMPs in rotating plasmas for DIII-D and ITER parameters.

## 2. Reduced MHD model with RMPs.

The non-linear cylindrical reduced MHD (RMHD) code [14] was adapted to take into account toroidal plasma rotation, resonant braking [6-8] and Neoclassical Toroidal Viscosity (NTV) [11-13]. The normalized as in [14] equations are:

$$\frac{\partial \psi}{\partial t} + v_z \frac{\partial \psi}{\partial z} + \nabla_{\parallel} \Phi = -\eta j \quad (1)$$

$$\frac{\partial W}{\partial t} + v_z \frac{\partial W}{\partial z} + \nabla_{\parallel} j + [\Phi, W] = \nu_{\perp,0} \nabla^2 W \quad (2)$$

$$\frac{\partial v_z}{\partial t} + v_z \frac{\partial v_z}{\partial z} + [\Phi, v_z] + \vec{\nabla}_{\parallel} p = S_v + \nu_{\parallel,0} \nabla^2 v_z + F_{RB} + F_{NTV} \quad (3)$$

$$\frac{\partial p}{\partial t} + v_z \frac{\partial p}{\partial z} + [\Phi, p] + k_{\perp} \nabla^2 p = S_p \quad (4)$$

Here  $\psi = \psi_0 + \tilde{\psi}$  - is a poloidal flux. Identifying equilibrium values with “eq” and perturbations with “~”, the total magnetic field is represented as follows:  $\vec{B} = \vec{B}_{eq} + \tilde{\vec{B}}$ ,  $\tilde{\vec{B}} = \left( \frac{1}{r} \frac{\partial \tilde{\psi}}{\partial \theta}; -\frac{\partial \tilde{\psi}}{\partial r}; 0 \right)$ ;  $\vec{B}_{eq} \approx B_0(0, b_{\theta,0}(r), b_{z,0})$ ;  $b_{z,0} \approx b_0 = 1$ ;  $b_{\theta,0}(r) = -\frac{1}{B_0} \frac{\partial \psi_0}{\partial r}$ . Other

variables are:  $\Phi$  - electrostatic potential,  $W = -\nabla^2 \Phi$  - vorticity,  $p$ -pressure,  $\vec{v} = \vec{v}_{\perp} + \vec{v}_{\parallel}$  - total velocity where the parallel to the equilibrium magnetic field component is approximated as:  $\vec{v}_{\parallel} = \vec{b}_{eq} (\vec{v}, \vec{b}_{eq})$ ,  $\vec{b}_{eq} = \vec{B}_{eq} / B_{eq}$ ,  $v_z \approx v_{\parallel,z}$ , and the poloidal velocity is approximated as:  $\vec{v}_{\perp} \approx -(\vec{\nabla} \Phi \times \vec{e}_z)$ ,  $k_{\perp}$  - diffusion coefficient,  $\nu_{\perp,0}, \nu_{\parallel,0}$  perpendicular and parallel viscosity  $j = -\nabla^2 \psi$  - toroidal current,  $B_0$  - is magnetic field on the axis. To derive the induction

equation (1) we used:  $(-\nabla \Phi - \frac{\partial \psi \vec{e}_z}{\partial t} - \eta \vec{J}) \cdot \vec{b}_{eq} \approx -(\vec{v}_{\perp} \times \vec{B} + \vec{v}_{\parallel} \times \tilde{\vec{B}}) \cdot \vec{b}_{eq}$ ;

$$\frac{b_{0,\theta} v_{\parallel,z}}{r} \frac{\partial \psi}{\partial \theta} = -v_{\parallel,z} \frac{\partial \psi}{\partial z}, \text{ where the cylindrical safety factor is: } q(r) = \frac{rb_{z,0}}{R_0 b_{\theta,0}}$$

$1/R_0 \partial_{\phi} \dots = \partial_z \dots$ . The equilibrium flow is given by  $\vec{v}_0 = (0, v_{\theta,0}, v_{z,0})$ ,  $v_{\theta,0} \ll v_{z,0}$ .  $S_{p,v}$  - represents sources that are adjusted to keep initial equilibrium profiles without RMPs. In the present modelling pressure terms were neglected by setting:  $p \sim 10^{-6}$ . The parallel gradient is:

$\nabla_{\parallel} \ldots = \partial \ldots / \partial z + [\ldots, \psi]$ ;  $[\Phi, \psi] = \vec{e}_z \cdot \nabla_{\perp} \Phi \times \nabla_{\perp} \psi$ . All lengths are normalized to the minor radius ( $a$ ). All variables are presented in Fourier series:  $\psi = \sum_{m,n=\pm\infty} \psi_{nm} e^{im\theta+inz/R_0} + c.c.$ ,  $n=0, m=0$

is the equilibrium value. The boundary conditions at  $r=1$  are zero for all perturbations except for the magnetic flux harmonic's amplitudes:  $\psi_{nm}|_{r=1} \approx \psi_{nm,sep}^{vac}$  which are approximated by the vacuum amplitudes calculated in the toroidal geometry [4]. Notice, that because of the much stronger magnetic shear in toroidal geometry, the amplitudes of the cylindrical harmonics at the edge were adjusted to satisfy edge islands overlapping for  $r>0.9$  (Chirikov parameter  $>1$ ) for the zero rotation case to correspond with this respect the vacuum modeling in a torus [4]. The resonant braking term due to  $\vec{j} \times \vec{B}$  forces in (3) is only taken into account for the mean flow ( $n=0, m=0$ ) as in [7-8]:

$$F_{RB}^{00} = \frac{-1}{2qR_0} \text{Im} \sum_{m,n \neq 0} m \left[ j_{nm} \psi_{nm}^* - \Phi_{nm} \left( \frac{\partial \Phi_{nm}^2}{\partial r^2} - \frac{1}{r} \frac{\partial \Phi_{nm}}{\partial r} \right)^* \right] \quad (5)$$

However, let us notice already that, for the typical RMP amplitudes modeled here, the resonant braking (5) typically localized near the resonant surfaces [6-8] is very small.

### 3. Modeling of NTV in DIII-D and ITER.

The expressions for the NTV force is taken from [11-13] in the form:

$$F_{NTV} = -\nu_{eff}^{||} b_{eff}^2 (V_{tor} - V_{tor}^{NC}) \approx -\alpha_{NTV}(r) (V_{tor} - V_{tor}^{NC}) \quad (6)$$

Here  $\nu_{eff}^{||}$  is the effective frequency and  $b_{eff}^2$  is the square of the effective magnetic perturbation calculated in Hamada coordinates in a specific way depending on the collisionality regime [11-13],  $V_{tor}$  is the toroidal velocity,  $V_{tor}^{NC}$  is the neoclassical toroidal velocity in a helically perturbed magnetic field [12]. Since the realistic toroidal geometry is very important for the NTV estimations [7-9], we stepped out from the self-consistency in RMHD modeling with NTV and used flux-averaged  $\alpha_{NTV}(r)$  calculated in toroidal geometry as input. Notice, that, unless noted, the magnetic perturbation in the NTV calculations was taken as in vacuum (see Sec.3). For the DIII-D case the parameters from discharge #127744 were used (Fig.1) ( $B_0=1.9T$ ,  $R_0=1.8m$ ,  $a=0.6m$ ,  $n=3$ ,  $I_{coil}=4.65kA$ , odd parity). The 9x3-rows RMP in-vessel ITER coils (Fig.2) were modeled by zero-thickness equally spaced frames with  $\sim 26^\circ$  toroidal width. The corners coordinates ( $R, Z$ ) in (m) for the top coil are: (7.71; 3.35); (8.53; 1.87); mid: (8.73; 1.75); (8.73; -0.5); bottom coil: (8.55; -0.62); (7.45; -2.49). The toroidal number in ITER coils spectrum was  $n=4$  produced by currents (in  $kA$ ) in the top-row: (-49.9; 45.675; -35.95; 21.9; -5.225; -12.1; 27.95; -40.45; 48.05); mid-row: (50; -47; 38.3; -25; 8.7; 8.7; -25; 38.3; -47) and bottom-row: (-42.4; 48.9; -49.5; 44.15; 33.45; 18.75; -1.75; -15.45; 30.8). The ITER H-mode scenario parameters are presented on Fig.3. The low collisionality 1/v- NTV regime is applicable [11-12] when  $q\omega_E < v_i/\varepsilon < \sqrt{\varepsilon}\omega_{ti}$ , here  $\varepsilon=r/R_0$ ,  $\omega_E \approx E_r/(rB_\phi)$  is the poloidal drift frequency,  $\omega_{ti} = V_{ti}/(R_0 q)$  is the ion transit frequency and  $V_{ti}$  is the ion thermal velocity. To estimate the radial electric field, the force balance was used:  $E_r = \nabla_r P_i / (eZ_i n_i) + V_\phi B_\theta - V_\theta B_\phi$  where the poloidal velocity is neoclassical:  $V_\theta = V_\theta^{neo} \approx 1.17/(Z_i B_\phi) dT_i/dr$  and  $v_i = 15.2/\sqrt{A} \ln \Lambda n_{(10^{19} m^{-3})} T_i^{-3/2} i_{(keV)}$  [15]. In the 1/v-regime:  $F_{NTV} = -\nu_{1/v}^{||} b_{1/v}^2 (V_z - V_{1/v}^{NC})$ ,  $V_{1/v(m/s)}^{NC} = 3.5/(Z_i B_\theta) (dT_{i,keV}/dr)$  is the neoclassical toroidal

velocity [12], where  $\nu_{1/v}^{\parallel} = \omega_i^2 / v_i$  is the effective frequency, and the effective perturbation:  $b_{1/v}^2 \approx 1.74q^2 \varepsilon^{3/2} \sum_{n>0} \sum_{m,m'=\pm\infty} n^2 (b_{nm} b_{nm'c} + b_{nms} b_{nm's}) W_{nmm'}$ , where  $b_{nm,s}$  are the harmonic amplitudes of the field perturbation strength:  $b \approx (\bar{B}_{eq} \cdot \tilde{\vec{B}}) / B_0^2$  in Hamada coordinates,

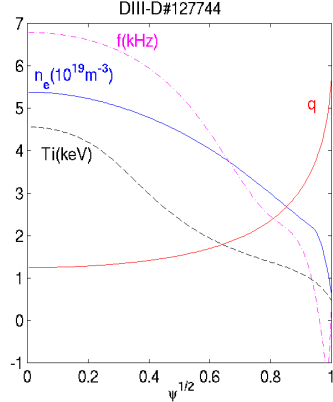


**Fig.1.** DIII-D shot #127744 parameters used for NTV estimations.

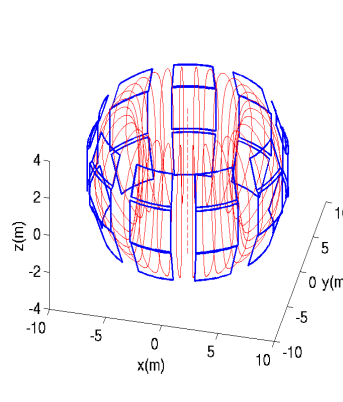


**Fig.2.** Sketch of ITER RMP coils (in blue) with plasma flux surfaces (in red).

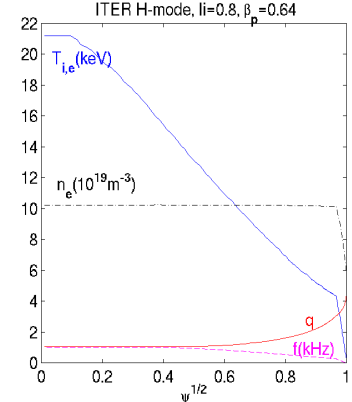


**Fig.3.** ITER H-mode parameters used for NTV estimations.

normalized to the magnetic field on the axis ( $B_0$ ). The total magnetic field strength [11-13] is:

$$B = \left( \bar{B}_{eq} + \tilde{\vec{B}}, \bar{B}_{eq} + \tilde{\vec{B}} \right)^{1/2} \approx B_{eq} + B_0 b. \quad \text{Introducing the label of the magnetic line: } \zeta^0 = q\theta^H - \zeta^H, \text{ where } (\theta^H, \zeta^H) \text{ are angles in Hamada coordinates, one can represent: } b = \sum_{n=\pm\infty} \sum_{m=\pm\infty} b_{nm} e^{-in\zeta^H + im\theta^H} = \sum_{n>0} A_n \cos(n\zeta^0) + B_n \sin(n\zeta^0), \text{ where: } A_n = \sum_{m=\pm\infty} b_{nm} \cos(\theta^H(m-nq)) + b_{nms} \sin(\theta^H(m-nq)); B_n = \sum_{m=\pm\infty} b_{nms} \cos(\theta^H(m-nq)) - b_{nm} \sin(\theta^H(m-nq)) \\ b_{nm} = \begin{cases} 2 \operatorname{Re}(b_{nm}), m \neq 0 \\ \operatorname{Re}(b_{nm}), m = 0 \end{cases}; b_{nms} = \begin{cases} -2 \operatorname{Im}(b_{nm}), m \neq 0 \\ -\operatorname{Im}(b_{nm}), m = 0 \end{cases} \quad (7)$$

The expressions for the weighting functions in  $1/v$ -regime are:

$$W_{nmm'} = \int_0^1 \frac{F_{nmc} F_{nm'c} dk^2}{E(k) - (1 - k^2) K(k)}; F_{nmc}(k) = 2 \int_0^{2\arcsin k} \sqrt{k^2 - \sin^2(\theta/2)} \cos(\theta(m-nq)) d\theta \quad (8)$$

The complete elliptic integrals of the first and second kind are defined as:

$$E(k) = \int_0^{\pi/2} (1 - k^2 \sin^2 \theta)^{1/2} d\theta; K(k) = \int_0^{\pi/2} (1 - k^2 \sin^2 \theta)^{-1/2} d\theta. \quad \text{The perturbation spectrum } |b_{nm}|$$

(7) for DIII-D parameters is shown in Fig.4. The characteristic frequencies for DIII-D and ITER parameters are presented for ions and electrons in Fig.5-6. Here:  $A = 2; Z_i = 1; \ln \Lambda = 20$ . Notice that electrons are in  $1/v$ -regime (Fig.6). Since for the ions mainly:  $q\omega_E > \nu_i / \varepsilon$  (Fig.5), the  $v$ -regime is expected. Notice that the radial electric field is the most uncertain in these estimations. For  $v$ -regime we used [13] that includes the boundary between trapped and passing particles corrections compared to the studies [11-12]:  $F_{NTV} = -\nu_v^{\parallel} b_v^2 (V_{tor} - V_v^{NC})$ , where:  $\nu_v^{\parallel} = \nu_i \omega_i^2 / \omega_E^2; V_v^{NC} = 0.92 / (Z_i B_0) (dT_{i,keV} / dr)$ ; (9)

$$b_v^2 = \sum_{n>0, m, m'=\pm\infty} (b_{nm} b_{nm'c} + b_{nms} b_{nm's}) W_{nmm'}^{(1)} + (b_{nm} b_{nm's} - b_{nms} b_{nm'c}) W_{nmm'}^{(2)}$$

$$W_{nmn'}^{(1)} = 0.045 \varepsilon^{-1/2} \int_0^1 dk^2 [E(k) - (1-k^2)K(k)] \left( \frac{\partial L_{nmn'}^{(1)}}{\partial k^2} + \frac{\partial L_{nmn'}^{(2)}}{\partial k^2} \right); \quad (10)$$

$$W_{nmn'}^{(2)} = 0.09 \varepsilon^{-1/2} \int_0^1 dk^2 [E(k) - (1-k^2)K(k)] \frac{\partial L_{nmn'}^{(1)}}{\partial k^2} \frac{\partial L_{nmn'}^{(2)}}{\partial k^2}; \quad (11)$$

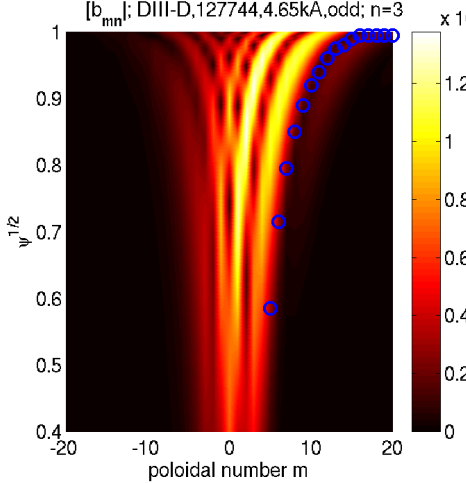


**Fig.4.** Magnetic perturbation spectrum  $|b_{nm}|$  (7) in Hamada coordinates for DIII-D #127744. Circles indicate the position of the resonant surfaces  $q=m/n$ .

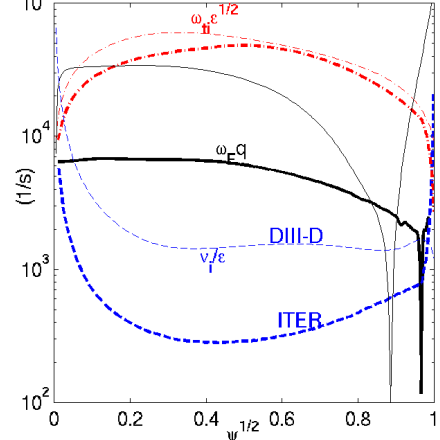


**Fig.5.** Characteristic ion transit (red), collision(blue) and toroidal drift frequency (black) for ITER (in bold) and DIII-D for parameters (Fig.1,3)

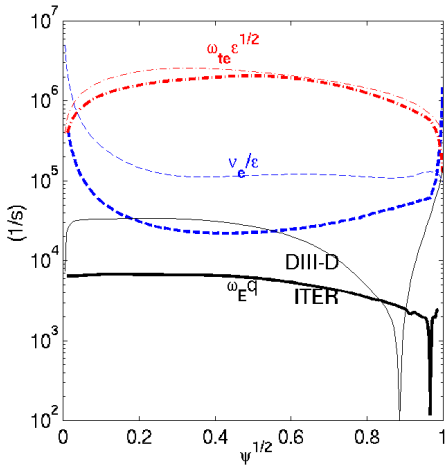


**Fig.6.** Characteristic electron transit, collision and toroidal drift frequencies for ITER (in bold) and DIII-D parameters presented on Fig.2-3.

$$L_{nmn'}^{(1)} = D_{nmn'} \frac{(1-e^{-\sigma(1-k^2)}) \cos(\sigma(1-k^2))}{K(k)}; \quad L_{nmn'}^{(2)} = D_{nmn'} \frac{e^{-\sigma(1-k^2)} \sin(\sigma(1-k^2))}{K(k)}; \quad (12)$$

$$D_{nmn'} = -2 \left\{ \int_0^{\pi/2} \frac{\cos[(m-nq)\theta(u)] du}{\sqrt{1-k^2 \sin^2(u)}} \right\}; \quad \theta(u) = 2 \arcsin(k \sin(u)); \quad \sigma \approx \sqrt{n} \left( \frac{v_d}{\ln(16/\sqrt{v_d})} \right)^{-1/2}; \quad v_d \approx \frac{4v_i}{\varepsilon \omega_E q};$$

The NTV damping time estimated for vacuum fields as  $t_{dam} \approx 1/(v_{eff}^{1/2} b_{eff}^2)$  is presented in Fig.7. To estimate the effective screening by the plasma rotation (dashed line in Fig.7) here we roughly set  $b_{nm}=0$  for  $r < r_{res}$  (see later in Sec 3). The present results indicate that the experimentally measured damping time is closer to  $1/v$  regime in DIII-D and the expected pure  $v$  regime [11-13] gives too small NTV to explain the observed global plasma braking. The more smooth transition between  $v$  and  $1/v$  regimes proposed in [17] partly removes this

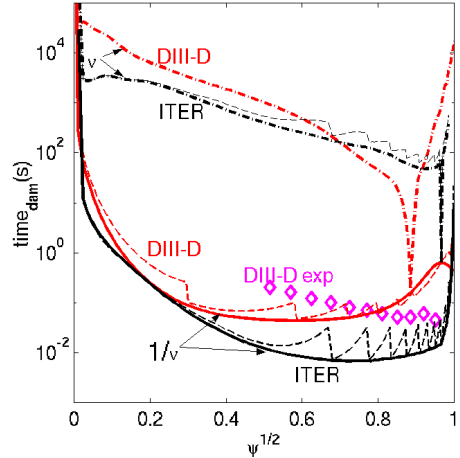


**Fig.7.** Damping time due to NTV in DIII-D 127744 and ITER. Dashed lines represent result with screening for resonant harmonics  $b_{nm}=0$  for  $r < r_{res}$

contradiction. However, the fact that the effective RMP strength seen by particle could be larger compared to the vacuum fields, as suggest 3D ideal plasma response modeling without islands formation [17], was not yet seen in the resistive MHD modeling [16], where more vacuum-like plasma response was obtained without plasma rotation. It is clear, that more self-consistent modeling of the resistive MHD plasma response on RMPs (including toroidal geometry, islands formation, plasma rotation and NTV) together with further dedicated experimental work, are still needed for more reliable predictions for ITER. The flux averaged profiles of NTV (6) used in RMHD code are presented in Fig.8. Certainly, the effect produced by RMPs on the rotation depends on the relative value of NTV compared to the intrinsic toroidal viscosity:  $\alpha_{NTV} / \nu_{\parallel,0}$ . The typical values in RMHD modeling were:  $\nu_{\perp,0} = 0.01$  corresponding to the strong damping of the mean poloidal flow [6-8] and  $\nu_{\parallel,0} = 3.10^{-7} - 10^{-6}$  corresponding roughly to the experimental toroidal viscosity ( $\sim$ few  $m/s^2$ ), the NTV in the  $v$ -regime (Fig.8) does not produce any noticeable rotation braking in the RMHD modelling and hence these results are not presented here.

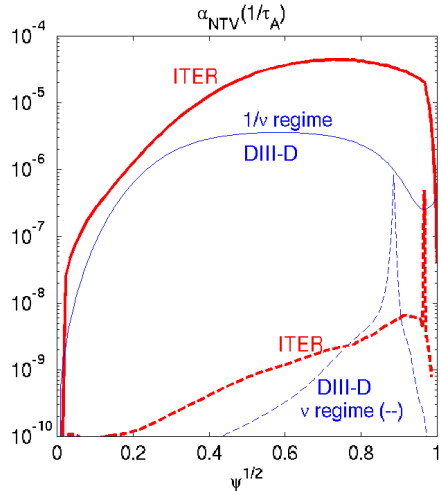


**Fig.8.** Normalized coefficient in (6) used in RMHD code (Sec.3) estimated for vacuum fields.

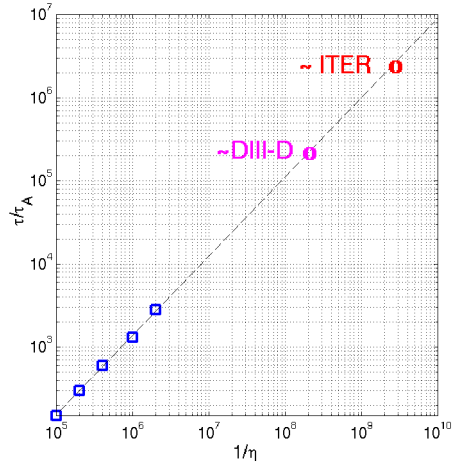


**Fig.9.** Normalized RMP penetration time to the top of the pedestal ( $r \sim 0.9$ ) of the harmonic  $m/n=9/3$  as a function of normalized  $(1/\eta)$ .  $\eta = \text{const}$ .

### 3. RMHD modeling results.

The first step in this study was to estimate the single harmonic penetration without rotation. The resulting flux perturbation  $|\psi_{n=-3,m=9}|$  on the surface  $q_{(r=0.9)} = |m/n|$  can be fitted by the formula:  $\psi_{nm}^{pl} \approx \psi_{nm}^{vac} (1 - 0.99 e^{-t/\tau})$ . The normalized on  $\tau_A$  penetration time  $\tau$  is presented as a function of the normalized  $\eta^{-1}$  (here  $\eta(r) = \text{const}$ ) on Fig.9. The values at the top of the pedestal are  $\tau \sim 600ms$  for ITER ( $T_{ped} = 4keV, \tau_A \sim 3.10^7 s$ ) and  $\tau \sim 60ms$  for DIII-D ( $T_{ped} = 2keV, \tau_A \sim 3.510^6 s$ ). In the following RMHD runs we adopted a more realistic resistivity profile:  $\eta = \eta_{pl} \eta_{vac} / (\eta_{pl} + \eta_{vac})$ ,  $\eta_{vac} = 0.1$ ,  $\eta_{pl} = \eta_0 (p / p_0)^{-3/2}$  which mimics the  $\sim T_e^{-3/2}$  temperature dependence. The pressure profile was typical for the H-mode scenario with an Edge Transport Barrier (ETB) at  $r > 0.9$ . Let us notice here that for  $n=3, n=4$  and the parabolic equilibrium toroidal current profile used here, no RMP amplification was observed in the present modelling. The rotation profile was taken parabolic with a central value  $V_0$ . The screening of magnetic islands due to the rotation is stronger at stronger rotation (Fig.10) and lower resistivity (Fig.11) as it is expected from theory [6]. The rotating plasma response on RMP mainly consists in the generation of a current layer on the resonant surface [6-7,16].

The results (Fig.10-11) confirm the predictions [6] for the *visco-resistive* linear regime:  $\psi_{mn}^{pl}/\psi_{mn}^{vac}|_{res} \sim \eta^{5/6}/V_0$ . Notice in Fig.12 that with rotation  $\psi_{mn}^{pl} \approx 0$  for  $r < r_{res}$  justifying the approximation for the screened harmonics amplitudes used in Sec 2.

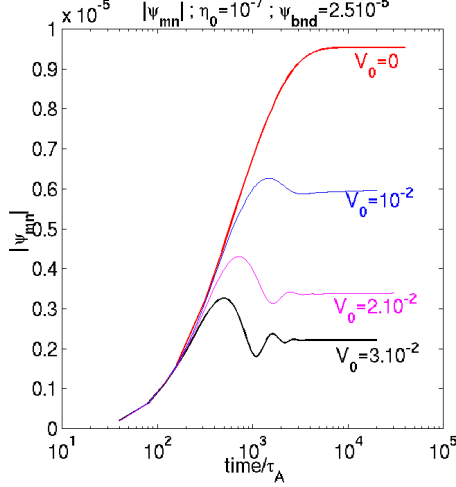


**Fig.10.** Time dependence of  $|\psi_{n=-3,m=9}|$  on the resonance surface  $r_{res}=0.9$  in the rotation  $V_0$  (in  $V_A$ ) scan.

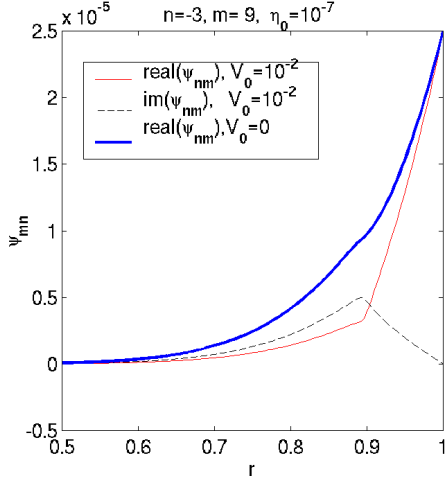


**Fig.12.** Flux perturbation profile at zero rotation  $V_0=0$  and with rotation  $V_0=10^{-2} V_A$ .

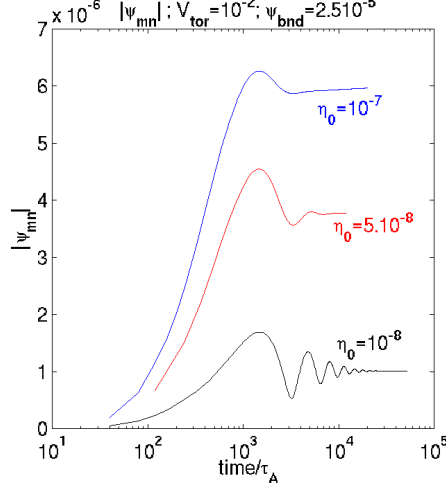


**Fig.11.** Time dependence of  $|\psi_{n=-3,m=9}|$  on the resonance surface  $r_{res}=0.9$  in the resistivity scan at  $V_0=10^{-2} V_A$ .

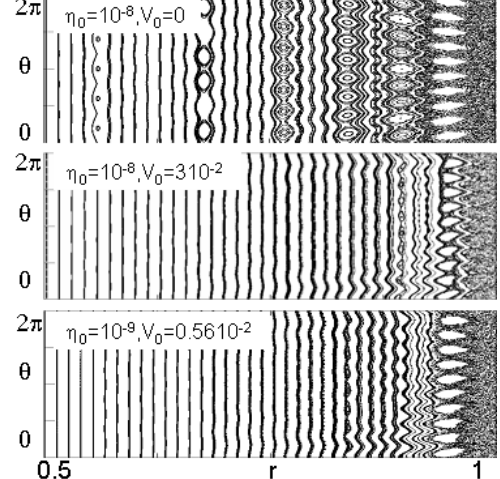


**Fig.13.** Screening central islands by rotation for DIII-D and ITER-like parameters.

The magnetic topology resulting from RMHD with rotation and  $F_{NTV}=0$  for the RMP spectrum  $\psi_{n,m=5:11}(r=1)=[9_{m=5};8_{m=6};...3_{m=11}]\cdot 10^{-5}$ ,  $n=-3$  ( $n < 0$  is a convention in the RMHD code), is presented in Fig.13. Notice that  $V_0=3\times 10^{-2}$  ( $\sim 10$  kHz),  $\eta_0=10^{-8}$  correspond to a DIII-D-like and  $V_0=0.56\times 10^{-2}$  ( $\sim 1$  kHz)  $\eta_0=10^{-9}$  to ITER-like plasma parameters. One can see that in both cases the central islands are screened, but still overlap for  $r>0.9$ . As it was shown by a number of the numerical tests (not presented here), the simplified equation  $\partial v_z/\partial t \approx S_v + v_{\parallel,0}\nabla^2 v_z - \alpha_{NTV,1/v}(v_z - V_{1/v}^{NC})$  leads to the toroidal rotation profile time evolution very close to the full RMHD modeling (1-4) at strong NTV ( $\alpha_{NTV}/v_{\parallel,0} \gg 1$ ). This permits to reduce significantly the time consuming numerical solution (1-4) with a typical time step  $\sim 0.1 \tau_A$  until the stationary rotation profile is reached ( $\sim 2.10^6 \tau_A$ ). Notice that the stationary rotation with NTV in  $1/v$ -regime (Fig.14) is in the counter direction (here negative) and close to the neoclassical value [12]. Notice also that similar to these numerical results, a spin

-up in the counter direction was experimentally observed on DIII-D with the I-coils at slow intrinsic co- or counter rotation [10]. The magnetic topology resulting from the RMHD modeling with NTV is presented in Fig.15 at different times (in  $\tau_A$ ) for ITER-like parameters ( $n = -4; m = 8:14; \psi_{r=1}^{nm} = 3.510^{-5}; \eta_0 = 10^{-8}$ ;  $\nu_{0,\parallel} = 3.10^{-7}$ ;  $\alpha_{NTV,max} = 2.10^{-5}$ ). Screening of RMPs is independent on the direction of the rotation (co- or counter) (Fig.15), however, notice that central islands can reappear when locally  $V_{tor} \sim 0$  ( $t = 5.610^4 \tau_A$ ).

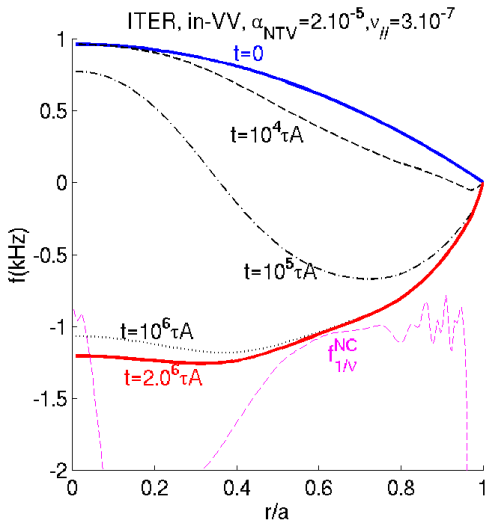


**Fig.14.** Rotation profile with NTV produced by ELM coils in 1/v regime in ITER (Fig.8). Neoclassical toroidal frequency (in magenta):  $f_{1/v}^{NC} = V_{1/v}^{NC} / (2\pi R_0)$

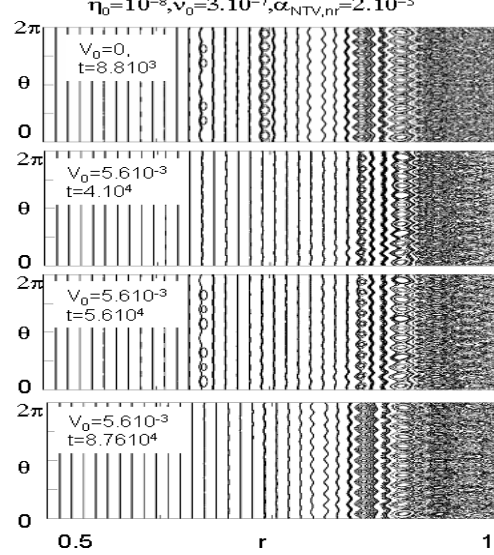


**Fig.15.** Poincare plots from RMHD code for ITER-like parameters with NTV in 1/v regime at different times (Fig.14).

#### 4. Conclusions and discussion.

The MHD response to RMPs in a rotating plasma was estimated for DIII-D and ITER. The effective screening of the central magnetic islands by plasma rotation and the pedestal region ergodisation are predicted. Non-resonant helical harmonics ( $q \neq m/n$ ) are not influenced by plasma rotation in modelling. The resonant ( $q=m/n$ ) harmonic's penetration time scales roughly with Lindquist number ( $\sim \eta^{-1}$ ). If the “1/v” NTV low collisionality regime [11-12] is dominant in ITER, the counter rotation close to the neoclassical estimations [12] is predicted for ITER similar to DIII-D observations at slow intrinsic rotation [10]. Further experimental validation and NTV modelling including MHD rotating plasma response is certainly needed for more reliable predictions of the rotation profile in ITER with RMP coils.

#### References:

- [1]R. Hawryluk et al This conference IT/1-2
- [2]T.E. Evans et al Nucl. Fusion **48** (2008) 024002
- [3]Y. Liang et al Phys Rev Letters **98** (2007) 265004
- [4]M. Becoulet et al. Nucl. Fusion **48** (2008) 024003
- [5]M. Schaffer et al Nucl. Fusion **48** (2008) 024004
- [6]R. Fitzpatrick Phys of Plasm **5** (1998) 3325
- [7]Y. Kikuchi et al PPCF **48**(2006)169
- [8]E. Lazzaro et al Phys of Plasm **9**(2002)3906
- [9] W.Zhu et al Phys Rev Lett **96**(2006) 225002
- [10]A. Garofalo et al Phys Rev Lett, accepted 2008
- [11]K. Shaing Phys. Plasm**10** (2003) 1443 Phys of Plas **14** (2007) 049903. (Erratum paper).
- [12]A. Cole et al Phys of Plasm **15**(2008)056102
- [13]K. Shaing et al Phys. Plasm **15**(2008) 082506
- [14]G. Huysmans Phys Rev Lett **87**(2001)245002
- [15]J. Wesson,Tokamaks, Oxford,2004
- [16]E. Nardon et al Phys of Plasm **14**(2007)092501
- [17] J-K Park et al This conference EX/5-3Rb